Probing the dynamics of Cu nanoparticle growth inside metal-organic frameworks upon electron beam irradiation

Yuri A. Mezenov, Stéphanie Bruyere, Nikita K. Kulachenkov, Andrei N. Yankin, Sergey S. Rzhevskiy, Pavel V. Alekseevskiy, Venera D. Gilemkhanova, Semyon V. Bachinin, Vyacheslav Dyachuk, Andrei A. Krasilin, et al.

Probing the dynamics of Cu nanoparticle growth inside metal-organic frameworks upon electron beam irradiation

Yuri A. Mezenov[a], Stéphanie Bruyere[b], Nikita K. Kulachenkov[a], Andrei N. Yankin[a], Sergey S. Rzhevskiy[a], Pavel V. Alekseevskii[a], Venera D. Gilemkhanova[a], Semyon V. Bachinin[a], Vyacheslav Dyachuk[a,c], Andrei A. Krasilin[a,d], Julien Zollinger[b], Thierry Belmonte[b], Alexandre Nominé[a,b], Valentin A. Milichko[a,b]

[a] Department of Physics and Engineering, ITMO University, Kronverksky Pr. 49, St. Petersburg, 197101, Russia

[b] Université de Lorraine, CNRS, IJL, F-54000, Nancy, France

[c] A.V. Zhirmunsky National Scientific Center of Marine Biology, Far Eastern Branch, Russian Academy of Sciences, Vladivostok, 690041, Russia

[d] Ioffe Institute, Politekhnicheskaya 26, St. Petersburg, 194021, Russia

ABSTRACT

Metal-organic frameworks (MOFs) represent a unique platform for fabrication of nanoparticles (NPs) of diverse composition and crystallinity. The growth of NPs from constituent parts of MOFs is usually initiated by external stimuli such as temperature, light and electron irradiation. Herein, the kinetics and NP growth mechanisms remain unexplored. Here, we utilized electron irradiation to initiate the nucleation and growth of crystalline Cu NPs of tunable size from several nanometers to hundreds of nanometers inside MOF as a precursor. Simultaneously, the process of the NPs growth, captured in real time using transmission electron microscope, demonstrates the evolution of their size, shape and spatial distribution. We also analyze the NP growth by the classical kinetic theory taking into account a phase transformation. Our results contribute to crystal engineering and developing of functional MOF-based nanocomposites.

1. Introduction

Metal-organic frameworks (MOFs) hold a special place in material science and crystal engineering [1]. Over the last two decades, such materials have attracted increasing attention of researchers in chemistry, biology and physics [2–4]. Belonging to a class of porous coordination polymers, MOFs consist of metal-containing nodes connected by multi-topic organic linkers. As a result, they are characterized by hierarchical structure with high porosity, chemical versatility and flexibility, which allow them to demonstrate advanced adsorption, catalytic, mechanical and radiative properties [2–7].

The development of synthetic approaches and post-processing methods brings MOFs closer to commercial applications [8]. On the one hand, the compatibility of MOFs with chemical vapour deposition technology [9], plasma synthesis [10], and thin film growth [11] supports their integration into microelectronic devices. On the other hand, the post-processing of MOFs by heat [12], light [13,14] and electron irradiation [15–18] highlights their application as optical glasses and active optical elements in nanophotonics. Indeed, such post-processing initiates the deformation of framework backbone and breaking of chemical bonds [19] leading to formation of amorphous glassy compounds [12], nanocomposites [20] and nanoparticles (NPs) with different optial properties [13,14,21]. Herein, compared to investigating mechanisms of nucleation and growth of initial MOFs [1] and different inorganic NPs [22–24], the kinetics of formation of NPs from constituent parts of MOFs remain unexplored.

In this work, we report on exposure of MOFs to focused electron beam (e-beam) of transmission electron microscope (TEM, Fig. 1a) to initiate the nucleation and growth of crystalline metallic NPs with tunable size from ⍰2 nm to ⍰100 nm. The process of the NPs growth, captured in real time, demonstrates the evolution of their size, shape and spatial distribution and can be analyzed by classical kinetic theory taking into account the phase transformation [23,24].

2. Results and discussion

As a model compound, we have utilized the commercially available HKUST-1, Basolite® C 300 produced by BASF (Fig. 1b). This is highly porous three-dimensional compound, Cu3BTC2, composed of Cu (II) ions and benzene-1,3,5-tricarboxylate (BTC) linkers [25]. HKUST-1 is also a representative class of MOFs that are easy to grow on different surfaces following a layer-by-layer approach [26], which makes it promising for applied research. Moreover, the compound has been recently investigated to reveal the mechanism of electron-induced decomposition and the reason for NPs formation [15–18].

The composition of HKUST-1 and its cubic space group Fm m have been confirmed by Raman spectroscopy and powder X-ray diffraction, respectively, in a recent article of ours [27]. TEM experiments on initiation and simultaneous analysis of the NPs growth have been carried out using MET - ACCEL ARM 200 F operating at 200 kV (emission 15 μA and various current density). For this, the powder of HKUST-1 has been placed on carbon TEM grids. Fig. 1d–k represents distinctive TEM micrographs captured in time with defferent magnification (60 and 80 k). In contrast to previous results [28,29], demonstrating that MOFs begin to lose their crystallinity when the cumulative electron dose reached 10–20 e− Å−2 with 300 kV-accelerated electron beam, the pores of HKUST-1 are not observable under our conditions. This is due to possible instability of the crystal structure under vacuum and electron irradiation with a higher electron density.

Comprehensive analysis of in situ e-beam initiation of the NPs growth inside the HKUST-1 single crystals and the dynamics of the growth reveal the following:

(i) Highly crystalline NPs can grow inside HKUST-1 under focused e-beam (Fig. 2). Energy dispersive X-ray (EDX) analysis with a JEOL Centurio, 1 sr detector, shows the exclusive presence of Cu within the NPs after electron irradiation (Fig. 3). This observation is confirmed by the fact that measured interplanar distances (<dhkl> = 0.207 ± 0.004 nm) are in excellent agreement with the (111) interplanar distance of Cu (d111 = 0.2087 nm). Based on the previous results on the effect of e-beam on the chemi cal bounding of MOFs [15–18] and similar reason for growth of Pt and Au NPs from organometallic precursors [30,31], the possibility of the growth of the NPs from the constituent parts of HKUST-1 is due to breaking of bonds between copper and organic part. Moreover, the growth of pure Cu NPs instead of its oxide form is explained by a lower oxidation potential of Cu and relatively weak Cu COO bond energy, which promote the metallic state [15].

(ii) The growth process begins mainly on the MOF's surface, and then propagates throughout the whole volume (SI, video 3). It should be noted that full conversion of MOF to the nanocomposite can be observed after several minutes (Fig. 4a and b). Herein, the time threshold of the detection of small NPs (5 and 11 s for 60 and 80k magnification) in TEM is observed (Fig. 5a and b), which confirms the relatively slow free Cu atom movement process to form a nucleus of 1−3 nm in diameter with other free atoms.

(iii) The rates of the NPs growth (Fig. 1d–k) strongly depend on the parameters of focused e-beam, such as magnification (60 and 80 k at a constant electron energy), determining the electron density. Indeed, an increase of magnification from 60 to 80k leads to a 7-fold increase in rate (Fig. 5a and b), i.e. 9-nm NP can be created in 40 and 5.5 s, respectively.

(iv) Increase in electron density (magnification) also results in the growth of NPs with larger diameter until the saturation of this process is observed (Fig. 5a and b). The maximal diameters of the NPs observed are ~50 and ~144 nm after 2 min e-beam irradiation with 60 and 80 k magnification, respectively.

(v) The evolution of the number of Cu NPs does not follow a monotonic trend over the e-beam exposure time (Fig. 5a and b). This reflects the coexistence of two phenomena: NPs nucleation and growth, that contribute to increasing their number, and NPs coa lescence that decreases their surface energy, which, in turn, decreases the number of the NPs with an increase of their size. The competition between these two phenomena is indeed more noticeable for smaller size of NPs (i.e. beginning of e-beam exposure) which are closer and more mobile than the larger one, and therefore, more subject to coalescence (Fig. 4c and d). For larger NPs, the surface-to-volume energy ratio becomes much more favorable to the volume energy and therefore to the NPs growth. In other terms, a newly formed free Cu atom is much more likely to be adsorbed by large NPs rather than to form a nucleus with other free atoms, and even in this case, the phenomenon of Ostwald ripening would rapidly make the nucleus be absorbed by the larger NPs, probably before the nucleus could even be detected.

(vi) Finally, the shape of the growing NP can also vary due to coalescence (Fig. 4e and f) [24]. As a result, spherical NPs with ⍰100 nm in diameter can be observed. In turn, smaller NPs demonstrate well-defined faceted shape that is commonly encountered for crystalline Cu NPs [32]. Since the larger NPs come from the assembling of several smaller NPs, they are more likely to be polycrystalline and therefore closer to an overall spherical shape. Smaller NPs are more likely to be single crystals and therefore the growth is more likely to follow lower energy directions.

Based on experimental results, we then model the kinetic of phase transformation. The nucleation and growth can be modelled by either the Gualtieri or Johnson-Mehl-Avrami-Kolmogorov (JMAK) models. Van Vleet et al. have demonstrated that the Gualtieri model is more ap propriate for the prediction of MOF nucleation and growth [1]. However, in the present case, the phase transformation corresponds

to a solid – solid one (MOF → Cu NPs + glassy phase). Moreover, by separating the nucleation and the growth process, the Gualtieri model requires input parameters of both steps. In the present case, the determination of nucleation input parameters is challenging due to detecting of the NPs with a minimum diameter of ⍰2 nm (Fig. 5a and b). Hence, we model the growth of Cu NPs using classical growth theory with JMAK equation [33]:

$$V^{NP}(t) = V_{max}^{Cu}(1 - \exp(-Kt^n)) \quad (1)$$

Where V^{NP} is the volume of Cu NP formed, V^{Cu}_{max} the maximum volume of Cu that can be formed, K and n the JMAK coefficients [23]. The first JMAK coefficient K is expressed by:

$$K = \frac{\pi \dot{N} \dot{r}^3}{3} \quad (2)$$

with dN/dt the nucleation rate (number of new nuclei per unit of volume per unit of time) and the linear growth rate. The later can be estimated from the experimental data as 0.22 nm s^{-1} and 1.25 nm s^{-1} for magnification of 60k and 80k, respectively (Figs. 5a and b, and S1). is estimated by the following equation [34]:

$$\dot{N} = \frac{\dot{r}}{d^4} \quad (3)$$

where d is the NP size (Fig. 5a and b). The parameter n accounts for the dimensionality of the transformation, the nucleation and the growth type (interface or diffusion limited). If the nucleation rate is nonzero and time-independent, n = m + 1, where m is equal to the dimensionality of the phase transformation for the interface-limited growth and one-half of the dimensionality for diffusion-limited growth [1]. Therefore, n has been chosen as equal to 4. This choice is first sustained by relatively small size of the NPs as compared to MOF crystal thickness varying from 0.1–10 µm (atomic force microscopy analysis, Fig. 1c), allowing a three dimensional growth of the crystals. Moreover, the evolution of the growth rate over time is linear (Fig. 5a and b), while parabolic evolution is expected for a diffusion-driven transformation. Rather than a diffusive process, the nucleation and growth of the NPs is attributed to breaking of the chemical bonding by the e-beam, leading to free Cu atoms precipitate into the NPs. This is supported by the fact that some NPs are facetted (Fig. 2d) which tends to show that, while Cu is growing, attachment kinetics is the limiting process. This can be illustrated by the JMAK model predicting a transformation time of 60 s and 25 s for 60 k and 80 k magnification, respectively (Fig. 5c and d). Therefore, it is possible to tune the quantity of Cu NPs before this time. Once the transformation is completed, the exposure time allows one to control the NP number and size thanks to the coalescence phenomenon. Fig. 5c and d also demonstrates the comparison of the experimental data and JMAK modelling of the time evolution of the NPs volume inside MOF, Eq. (1). As in case of the complicated process of growth of the crystals [23], one can observe a good agreement between the growth theory and the experimental results. This allows us to speculate on relatively classical microscopic-level processes of the crystalline NP growth inside MOF from its constituent parts due to breaking of the bonds between metal ions and organic linkers.

3. Conclusion

In summary, we experimentally analyzed and modeled the growth of crystalline Cu NPs of tunable size from ⍰2 nm to ⍰100 nm from the constituent parts of MOFs. For this, we utilized focused electron beam to initiate the nucleation and growth of NPs inside HKUST-1. The process of growth, captured in real time using transmission electron microscope, demonstrated the evolution of NP size, shape and

spatial distribution. The experimental results are in a good agreement with the classical kinetic theory of the NP growth using JMAK model taking into account a phase transformation. Our results contribute to crystal engineering and developing of functional MOF-based nanocomposites.

eclaration of Competing Interest

The authors declare that they have no known competing financial interests or personal relationships that could have appeared to influence the work reported in this paper.

Acknowledgements

This work is a part of joint Russian-French project “Hybrid photonics nanodevices” and is supported by The Ministry of Science and Higher Education of the Russian Federation (project No 14.587.21.0050 with unique identification RFMEFI58718×0050). ITMO University is acknowledged for providing access to the unique scientific instruments (AIST-NT TrIOS) for optical experiments.

References

[1] M J V Vleet, T Weng, X Li, J R Schmidt, In situ, time-resolved, and mechanistic studies of metal-organic framework nucleation and growth, Chem. Rev. 118 (2018) 3681–3721.

[2] H Furukawa, K E Cordova, M O'Keeffe, O M Yaghi, The chemistry and applications of metal-organic frameworks, Science 341 (2013) 1230444.

[3] K Lu, T Aung, N Guo, R Weichselbaum, W Lin, Nanoscale metal–Organic frameworks for therapeutic, imaging, and sensing applications, Adv. Mater. 30 (2018) 1707634.

[4] Y A Mezenov, A A Krasilin, V P Dzyuba, A Nominé, V A Milichko, Metal–organic frameworks in modern physics: highlights and perspectives, Adv. Sci. 6 (2019) 1900506.

[5] F X Coudert, J D Evans, Nanoscale metamaterials: Meta-MOFs and framework materials with anomalous behavior, Coord. Chem. Rev. 388 (2019) 48–62.

[6] V A Milichko, S V Makarov, A V Yulin, A V Vinogradov, A A Krasilin, E Ushakova, V P Dzyuba, E Hey-Hawkins, E A Pidko, P A Belov, Van der waals metal-organic framework as an excitonic material for advanced photonics, Adv. Mater. 29 (2017) 1606034.

[7] Y A Mezenov, N K Kulachenkov, A N Yankin, S S Rzhevskiy, P V Alekseevskiy, V D Gilemkhanova, S V Bachinin, V Dyachuk, V A Milichko, Polymer matrix incorporated with ZIF-8 for application in nonlinear optics, Nanomaterials 10 (2020) 1036.

[8] H Furukawa, U Müller, O M Yaghi, "Heterogeneity within order" in metal-organic frameworks, Angew. Chem. Int. Ed. 54 (2015) 3417.

[9] I Stassen, M Styles, G Grenci, H Van Gorp, W Vanderlinden, S De Feyter, P Falcaro, D De Vos, P Vereecken, R Ameloot, Chemical vapour deposition of zeolitic imidazolate framework thin films, Nat. Mater. 15 (2016) 304.

[10] X Jiang, Z Lin, X Zeng, J He, F Xu, P Deng, J Jia, X Jiang, X Hou, Z Long, Plasma-catalysed reaction Mn+ + L-H → MOFs: facile and tunable construction of metal-organic frameworks in dielectric barrier discharge, Chem. Commun. 55 (2019) 12192.

[11] A Bétard, R A Fischer, Metal–organic framework thin films: from fundamentals to applications, Chem. Rev. 112 (2012) 1055.

[12] R Gaillac, P Pullumbi, K A Beyer, K W Chapman, D A Keen, T D Bennett, F-X Coudert, Liquid metal–organic frameworks, Nat. Mater. 16 (2017) 1149.

[13] N K Kulachenkov, S Bruyere, S A Sapchenko, Y A Mezenov, D Sun, A A Krasilin, A Nominé, J Ghanbaja, T Belmonte, V P Fedin, E A Pidko, V A Milichko, Ultrafast melting of metal–organic frameworks for advanced nanophotonics, Adv. Funct. Mater. 30 (2020) 1908292.

[14] H Jiang, S Jin, C Wang, R Ma, Y Song, M Gao, X Liu, A Shen, G J Cheng, H Deng, Nanoscale laser metallurgy and patterning in air using MOFs, J. Am. Chem. Soc. 141 (2019) 5481–5489.

[15] B W Jacobs, R J T Houk, B M Wong, A A Talin, M D Allendorf, Electron beam synthesis of metal and semiconductor nanoparticles using metal–organic frameworks as ordered precursors, Nanotechnology 22 (2011) 375601.

[16] R J T Houk, B W Jacobs, F El Gabaly, N N Chang, A A Talin, D D Graham, S D House, I M Robertson, M D Allendorf, Silver cluster formation, dynamics, and chemistry in metal−organic frameworks, Nano Lett. 9 (2009) 3413.

[17] K Ahlenhoff, C Preischl, P Swiderek, H Marbach, Electron beam-induced surface activation of metal–organic framework HKUST-1: unraveling the underlying chemistry, J. Phys. Chem. C 122 (2018) 26658.

[18] K Ahlenhoff, S Koch, D Emmrich, R Dalpke, A Golzhauser, P Swiderek, Electron-induced chemistry of surface-grown coordination polymers with different linker anions, Phys. Chem. Chem. Phys. 21 (2019) 2351–2364.

[19] S Canossa, Z Ji, S Wuttke, Circumventing wear and tear of adaptive porous materials, Adv. Funct. Mater. (2020) 1908547.

[20] Y-Z Chen, B Gu, T Uchida, J Liu, X Liu, B-J Ye, Q Xu, H-L Jiang, Location determination of metal nanoparticles relative to a metal-organic framework, Nat. Commun. 10 (2019) 3462.

[21] L R Mingabudinova, A S Zalogina, A Krasilin, M I Petrova, P Trofimov, Y A Mezenov, E Ubyivovk, P Lönnecke, A Nomine, J Ghanbaja, T Belmonte, V A Milichko, Laser printing of optically resonant hollow crystalline carbon nanostructures from 1D and 2D metal–organic frameworks, Nanoscale 11 (2019) 10155.

[22] J Polte, Fundamental growth principle of colloidal metal nanoparticles – a new perspective, Cryst. Eng. Comm. 17 (2015) 6809–6830.

[23] A Schottelius, F Mambretti, A Kalinin, B Beyersdorff, A Rothkirch, C Goy, J Müller, N Petridis, M Ritzer, F Trinter, J M Fernández, T A Ezquerra, D E Galli, R E Grisenti, Crystal growth rates in supercooled atomic liquid mixtures, Nat. Mater. 19 (2020) 512–516.

[24] J Li, J Chen, H Wang, N Chen, Z Wang, L Guo, F L Deepak, In situ atomicscale study of particle-mediated nucleation and growth in amorphous bismuth to nanocrystal phase trensformation, Adv. Sci. 5 (2018) 1700992.

[25] S S-Y Chui, S M-F Lo, J P H Charmant, A G Orpen, I D Williams, A chemically functionalizable nanoporous material [Cu3(TMA)2(H2O)3]n, Science 283 (1999) 1148.

[26] J Liu, C Wöll, Surface-supported metal-organic framework thin films: fabrication methods, applications, and challenges, Chem. Soc. Rev. 46 (2017) 5730–5770.

[27] N K Kulachenkov, D Sun, Y A Mezenov, A N Yankin, S Rhzevskiy, V Dyachuk, A Nominé, G Medjahdi, E A Pidko, V A Milichko, Photochromic free MOF-based near-infrared optical switch, Angew. Chem. Int. Ed. (2020), doi:10.1002/ anie.202004293.

[28] Y Zhu, J Ciston, B Zheng, X Miao, C Czarnik, Y Pan, R Sougrat, Z Lai, C-E Hsiung, K Yao, I Pinnau, M Pan, Y Han, Unravelling surface and interfacial structures of a metal-organic framework by transmission electron microscopy, Nat. Mater. 16 (2017) 532.

[29] D Zhang, Y Zhu, L Liu, X Ying, C-E Hsiung, R Sougrat, K Li, Y Han, Atomic-resolution transmission electron microscopy of electron beam–sensitive crystalline materials, Science 359 (2018) 675.

[30] W Gao, P Tieu, C Addiego, Y Ma, J Wu, X Pan, Probing the dynamics of nanoparticle formation from a precursor at atomic resolution, Sci. Adv. 5 (2019) eaau9590.

[31] T Yao, Z Sun, Y Li, Z Pan, H Wei, Y Xie, M Nomura, Y Niwa, W Yan, Z Wu, Y Jiang, Q Liu, S Wei, Insights into initial kinetic nucleation of gold nanocrystals, J. Am. Chem. Soc. 132 (2010) 7696.

[32] Y Wang, A V Biradar, G Wang, K K Sharma, C T Duncan, S Rangan, T Asefa, Copper Nanoparticles and Their Catalytic Properties, Chem. Eur. J. 16 (2010) 10735.

[33] K A Jackson, Kinetic Processes, Wiley, 2004.

[34] J William, R Mehl, Reaction kinetics in processes of nucleation and growth, Trans. Metall. Soc. AIME 135 (1939) 416.

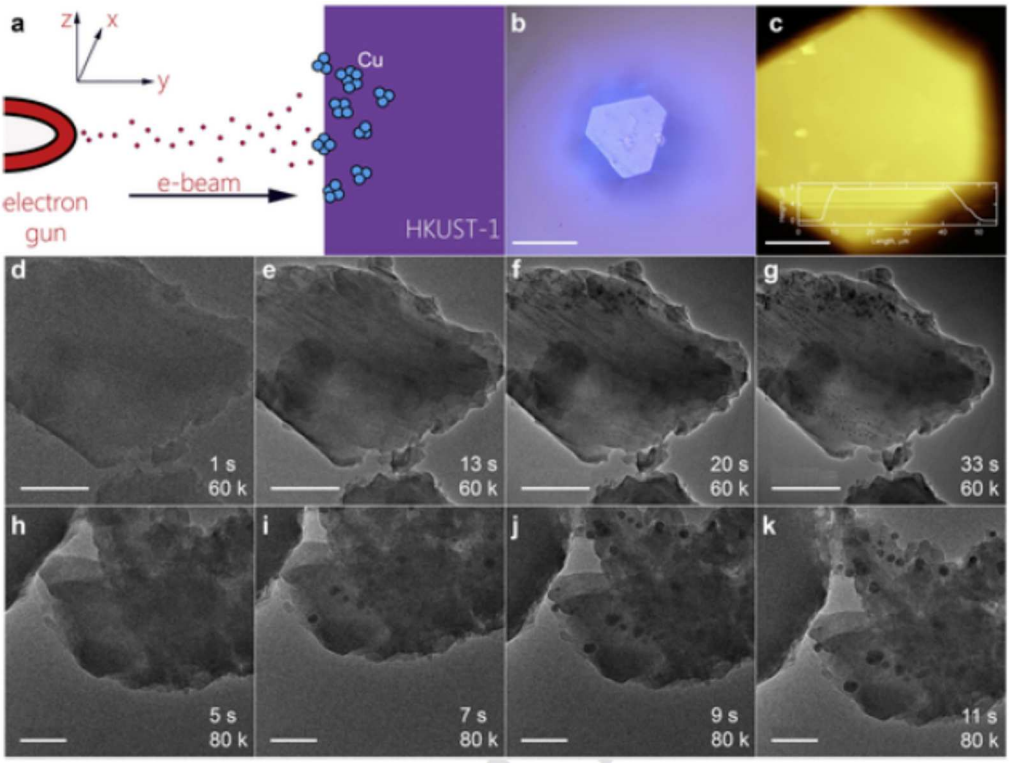

Fig. 1. (a) Schematic illustration of exposure of HKUST-1 single crystal to focused electron beam in TEM chamber for initiation and controll the growth of Cu NPs. (b,c) Optical image and atomic force microscopy (AFM) micrograph of HKUST-1 single crystal. Scale bars, 20 µm and 10 µm. Inset (c): AFM cross section of single crystal representing the heigth/length ration as 1/4,6. (d-g) Bright field TEM micrographs illustrating the dynamics of the NP growth inside HKUST-1 under magnification of 60 k. Scale bar, 200 nm. Corresponding video is in SI, video 1. (h-k) Dynamics of the NP growth inside HKUST-1 under magnification of 80 k. Scale bar, 100 nm. Corresponding video is in SI, video 2.

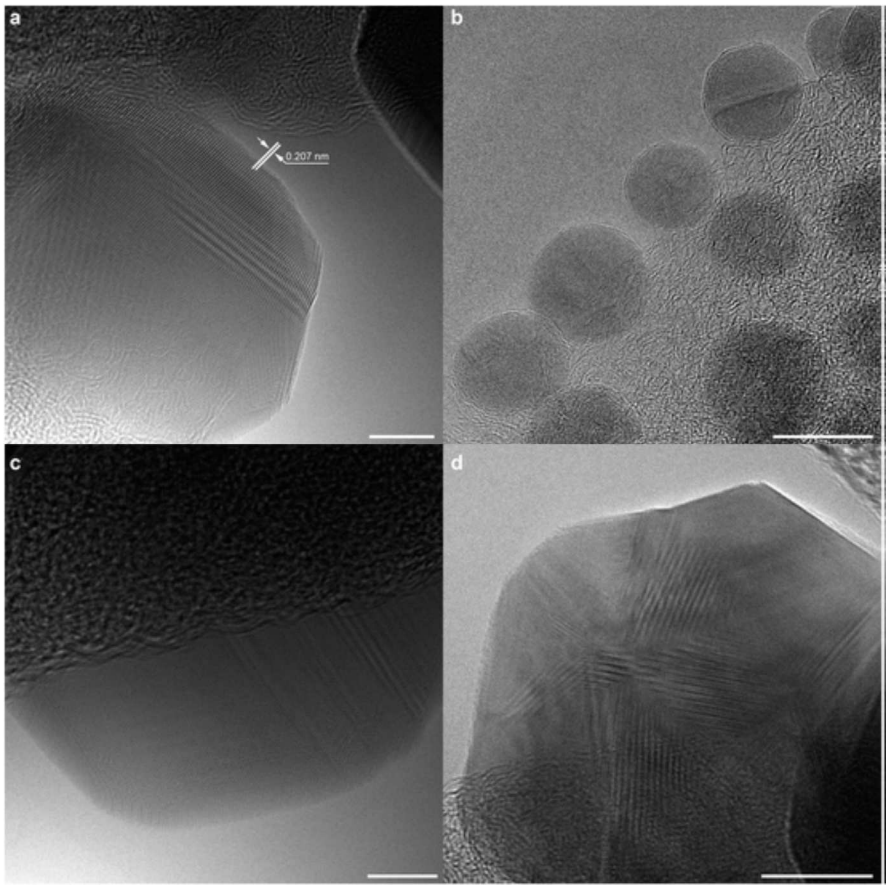

Fig. 2. (a–d) Bright field TEM micrographs of crystalline Cu NPs inside HKUST-1 obtained after 40 s of irradiation with 60 k magnification. (a) Interplanar distances measured < dhkl> = 0.207 ± 0.004 nm. Scale bars, 5 nm (a,c), and 10 nm (b,d).

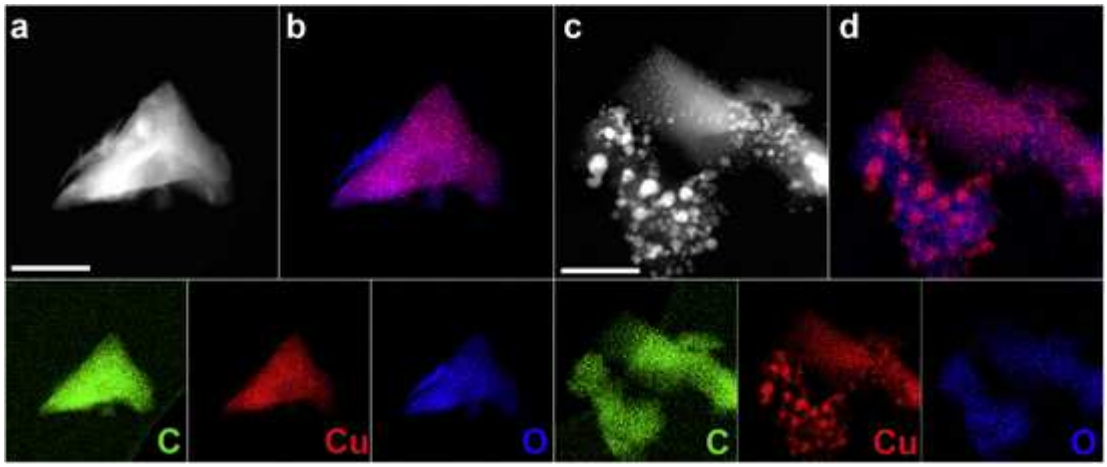

Fig. 3. (a,b) STEM-EDX map of HKUST-1 before focused e-beam irradiation confirming the homogeneous redistribution of the elements (C, Cu, O). Scale bar, 300 nm. (c,d) STEM-EDX map of HKUST-1 after focused e-beam irradiation. Cu NPs are represented in Red. Scale bar, 250 nm. Overlapping of Cu and O is represented in (b,d) demonstrating homogenity and inhomogeneity of Cu redistribution, respectively.

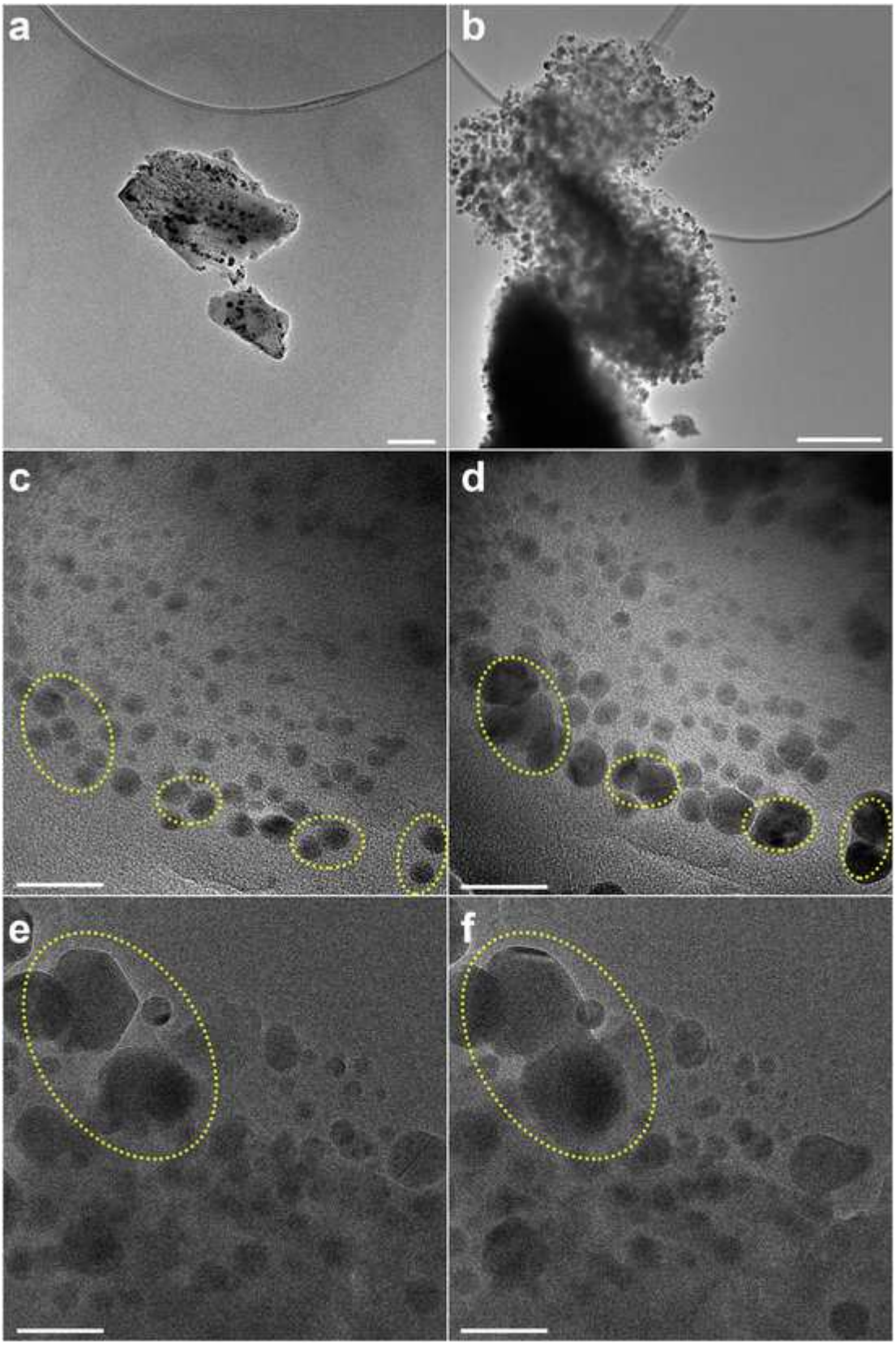

Fig. 4. (a,b) Bright field TEM micrographs of HKUST-1 after full conversion to the nanocomposite in 2 min upon focused e-beam with magnification of 60 k. Scale bars, 200 nm (a) and 500 nm (b). (c,d) Coalescence of the NPs from (c) in 30 s (d) upon focused e-beam with magnification of 60 k. Scale bar, 40 nm. (e,f) Changes of the NP shape (e) during coalescence in 4 s (f) upon focused e-beam with 80 k magnification. Scale bar, 60 nm.

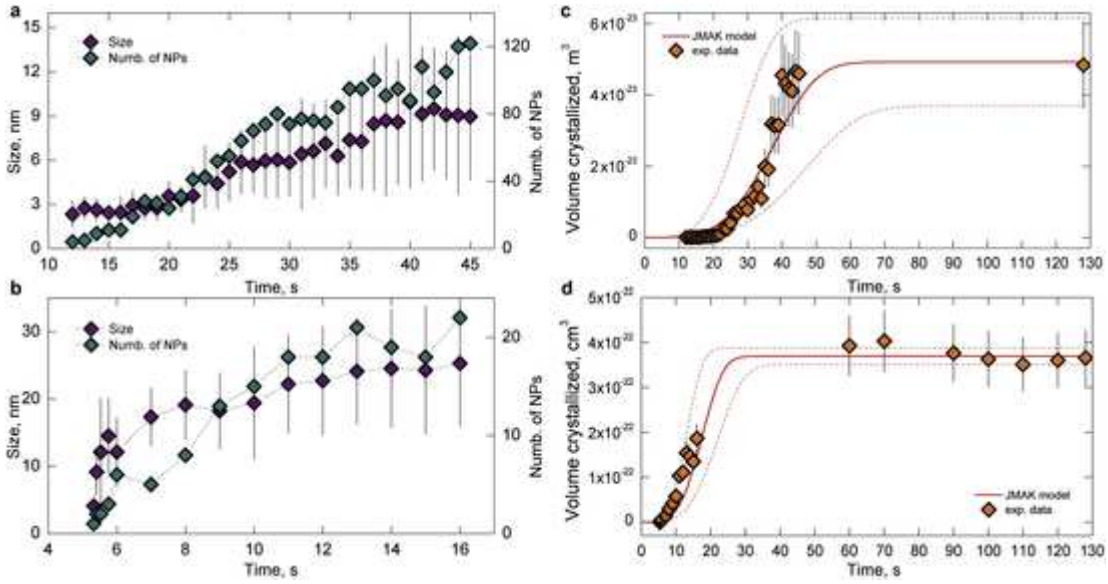

Fig. 5. (a,b) Analysis of the dynamics of the NP growth (size and the number of NPs) under focused e-beam irradiation with magnification of (a) 60 k and (b) 80 k. Irradiation started at t = 0 s, while the NPs with a minimal size of 2.5 nm have been detected by TEM in 11 and 5 s, respectively. (c,d) Time evolution of the Cu NP volume under e-beam irradiation with magnification of (c) 60 k and (d) 80 k. JMAK model (Eq. (1)) represents the red curve, while experimental data (the volume of growing NPs) are represented in squares. Dashed lines are the error of the JMAK model based on the correct analysis of the volume of MOF and the NPs